HHS Public Access

Author manuscript

Biomaterials. Author manuscript; available in PMC 2015 June 01.

Published in final edited form as:

Biomaterials. 2014 June ; 35(19): 5162–5170. doi:10.1016/j.biomaterials.2014.03.014.

Molecular imaging for assessment of mesenchymal stem cells mediated breast cancer therapy

Liang Leng[a,b,1], **Yuebing Wang**[a,1], **Ningning He**[a], **Di Wang**[a], **Qianjie Zhao**[a], **Guowei Feng**[a], **Weijun Su**[a], **Yang Xu**[a], **Zhongchao Han**[c], **Deling Kong**[b], **Zhen Cheng**[d], **Rong Xiang**[a], and **Zongjin Li**[a,b,*]

Zongjin Li: zongjinli@nankai.edu.cn

[a]Nankai University School of Medicine, Tianjin, China

[b]The Key Laboratory of Bioactive Materials, Ministry of Education, Nankai University, College of Life Science, Tianjin, China

[c]State Key Lab of Experimental Hematology, Institute of Hematology and Blood Diseases Hospital, Chinese Academy of Medical Sciences, Tianjin, China

[d]Department of Radiology, Stanford University School of Medicine, Stanford, CA 94305, USA

Abstract

The tumor tropism of mesenchymal stem cells (MSCs) makes them an excellent delivery vehicle used in anticancer therapy. However, the exact mechanisms of MSCs involved in tumor microenvironment are still not well defined. Molecular imaging technologies with the versatility in monitoring the therapeutic effects, as well as basic molecular and cellular processes in real time, offer tangible options to better guide MSCs mediated cancer therapy. In this study, an in situ breast cancer model was developed with MDA-MB-231 cells carrying a reporter system encoding a double fusion (DF) reporter gene consisting of firefly luciferase (Fluc) and enhanced green fluorescent protein (eGFP). In mice breast cancer model, we injected human umbilical cord-derived MSCs (hUC-MSCs) armed with a triple fusion (TF) gene containing the herpes simplex virus truncated thymidine kinase (HSV-ttk), renilla luciferase (Rluc) and red fluorescent protein (RFP) into tumor on day 13, 18, 23 after MDA-MB-231 cells injection. Bioluminescence imaging of Fluc and Rluc provided the real time monitor of tumor cells and hUC-MSCs simultaneously. We found that tumors were significantly inhibited by hUC-MSCs administration, and this effect was enhanced by ganciclovir (GCV) application. To further demonstrate the effect of hUC-MSCs on tumor cells *in vivo*, we employed the near infrared (NIR) imaging and the results showed that hUC-MSCs could inhibit tumor angiogenesis and increased apoptosis to a certain degree. In

*Corresponding author. Nankai University School of Medicine, 94 Weijin Road, Tianjin 300071, China. Tel.: +86 22 23509332; fax: +86 22 23509505.

[1]These two authors contributed equally to this work.

Competing interests: None.

Contributorship statement: ZL was the principal investigators and take primary responsibility for the paper. LL, ZL, YW, NH, RX, DK, ZH and ZC conceived and designed the experiments. LL, YW, NH, DW, WS, GF and YX performed the experiments. LL, YW and YX analyzed the data. ZL, LL and ZC wrote the paper.

Appendix A. Supplementary data: Supplementary data related to this article can be found at http://dx.doi.org/10.1016/j.biomaterials.2014.03.014.

conclusion, hUC-MSCs can inhibit breast cancer progression by inducing tumor cell death and suppressing angiogenesis. Moreover, molecular imaging is an invaluable tool in tracking cell delivery and tumor response to hUC-MSCs therapies as well as cellular and molecular processes in tumor.

Keywords

Mesenchymal stem cells (MSCs); Molecular imaging; Bioluminescence imaging (BLI); Near infrared (NIF) imaging; Cancer therapy

1. Introduction

Mesenchymal stem cells (MSCs) are multipotent cells that can be derived from a variety of tissues or organs, including bone marrow, adipose, placenta and umbilical cord [1]. With their capacity of tumor-specific tropism, MSCs have been considered to be attractive vehicles for delivering therapeutic agents toward tumor sites [2–5]. Several therapeutic strategies based on the local production of biological agents in tumors by gene-manipulated MSCs have been developed and exhibit potent antitumor activity [6,7]. Engineered MSCs with herpes simplex virus thymidine kinase (HSV-ttk), interferons (IFNs), interleukins (ILs), apoptosis inducers (e.g. TRAIL) or oncolytic viruses have manifested selective tumor repression [8–11]. Compared to other vehicles and/or delivery platforms as therapeutic carriers, MSCs provide exciting new possibilities for drug delivery used in tumor-targeted therapy.

Over the last decade, a variety of imaging technologies is being investigated as tools for cancer diagnosis, monitoring of response to cancer therapies and predicting of tumor response to available therapies as well as developing new drugs prior to clinical translation [12]. The successful clinical application of MSCs based tumor therapies needs non-invasive imaging approaches to monitor tumor progression and treatment outcome in real time [11,12]. Molecular imaging provides the possibility to visualize and monitor cellular and molecular processes, such as angiogenesis and apoptosis, in the living subjects for assessing the effect of MSCs on tumor progression [13,14].

Here, we hypothesize that real time *in vivo* imaging technologies could offer tangible options for better guiding MSCs delivery and monitoring antitumor activity of MSCs therapy. To test this hypothesis, we developed mouse model to analyze the behavior and efficiency of human umbilical cord-derived MSCs (hUC-MSCs) as a cellular vehicle for breast cancer therapy. We introduced dual reporter genes renilla luciferase (Rluc) and firefly luciferase (Fluc) for bioluminescence imaging of tumor progression and hUC-MSCs survival simultaneously within the same animal. Moreover, near infrared (NIR) fluorescence imaging method was applied to assess angiogenesis and apoptosis of tumor after hUC-MSCs therapy.

2. Materials and methods

2.1. Cell culture

Human breast cancer cell line MDA-MB-231 was purchased from ATCC (Manassas, VA, USA) and human umbilical cord mesenchymal stem cells (hUC-MSCs) were isolated and cultured as described [15,16]. MDA-MB-231 cells were grown in DMEM medium supplemented with 10% fetal bovine serum (FBS), 1% penicillin–streptomycin solution (Gibco, Rockville, MD), and 1% MEM non-essential amino acid solution (Gibco). hUC-MSCs were cultured with DMEM/F12 medium (Gibco) containing 10% FBS, 1% penicillin–streptomycin solution (Gibco), 10 ng/ml human recombinant epidermal growth factor (EGF; Gibco). For tracking transplanted cells *in vivo*, MDA-MB-231 cells were transduced with a self-inactivating lentiviral vector carrying an ubiquitin promoter driving firefly luciferase and enhanced green fluorescence protein (Fluc-eGFP) double fusion (DF) reporter gene. In addition, hUC-MSCs were labeled with a self-inactivating lentiviral vector carrying an EF1α promoter driving renilla luciferase (Rluc), red fluorescence protein (RFP), and herpes simplex virus truncated thymidine kinase (HSV-ttk) (Rluc-RFP-HSV-ttk) triple fusion (TF) reporter gene as described previously [9,11].

2.2. Tumor model

8–12 weeks old female Nu/Nu Nude mice (Laboratory Animal Center, the Academy of Military Medical Sciences, Beijing, China) were housed under standard laboratory conditions. All experimental procedures were conducted in conformity with institutional guidelines for The Care and Use of Laboratory Animals in Nankai University, Tianjin, China, and conformed to the National Institutes of Health (NIH) Guide for Care and Use of Laboratory Animals. Mice were injected with 1×10^6 MDA-MB-231 (Fluc-eGFP) cells into the fourth pair of mammary fat pad (day 0). After 13 days later, an intratumor injection of 1×10^6 MSC-TF cells was given on day 13, 18, 23. Twenty-four hours after hUC-MSC-TF cells injection, mice of the group were intraperitoneally injected with GCV (30 mg/kg) or PBS on days 14–17, 19–22, 24–27. Intratumor injection with PBS and ganciclovir (GCV; Keyi Pharmaceutic, Wuhan, Hubei, China) application for tumor bearing mice severed as control. Tumor development was evaluated by BLI of Fluc and hUC-MSC-TF cells were tracked by BLI of Rluc. At the end of experiment (day 30), all mice were euthanized and tumors were harvested for further analysis.

2.3. Optical imaging

Optical imaging was performed using IVIS 200 Imaging System (Xenogen Corporation, Hopkinton, MA). BLI of the fate of transplanted cells in living mice was done as described previously [17]. Imaging of Fluc and Rluc expression was used for assessing tumor development and hUC-MSC-TF cells' fate respectively. D-Luciferin (150 mg/kg; Biosynth International, Naperville, IL) was intraperitoneally injected into mice for evaluating Fluc expression, and each mouse was imaged for 1 s to 3 min. Coelenterazine (2.5 mg/kg; NanoLight Technology, Pinetop, AZ) was intravenously into mice for assessing Rluc expression. After injection of coelenterazine, mice were imaged for 2 min, immediately.

To monitor tumor angiogenesis and apoptosis status after hUC-MSC-TF cells administration, NIR fluorescence imaging of integrin $\alpha v\beta_3$ and annexin V was carried out with reagents IntegriSense™ 750 and Annexin-Vivo™ 750 (PerkinElmer, Waltham, MA). For IntegriSense™ 750 imaging, fluorescence signal was measured at excitation 755 nm (emission 775 nm) 24 h post-injection; similarly, fluorescence signal was obtained 2 h after Annexin-Vivo™ 750 imaging agent administration at excitation 755 nm (emission 772 nm) following the manufactures' recommendations.

2.4. Cell viability and bystander effect

To determine the effects of GCV on hUC-MSC-TF (Rluc-RFP-HSV-ttk), cells were seeded in 96-well plates (2×10^3/well) and treated with different doses of ganciclovir (GCV; Keyi Pharmaceutics, Wuhan, Hubei, China) (0–40 μg/ml) 24 h after plating. Cell viability was assessed at 48 h post GCV treatment by Cell Counting Kit-8 (CCK-8) (Dojindo). To investigate the time courses survival of hUC-MSC-TF cells after GCV treatment (40 μg/ml) over time, CCK-8 assay was carried out at day 1, day 2 and day 3. To assess bystander effect, different proportions hUC-MSC-TF cell were mixed with MDA-MB-231 (Fluc-eGFP) cells in 24-well plates and treated with GCV (40 μg/ml) after plating. After 2 days, the survival of MDA-MB-231 cells was evaluated by Fluc expression using IVIS 200 Imaging System (Xenogen Corporation). Moreover, to determine the time course of bystander effects, hUC-MSC-TF cells were mixed with MDA-MB-231 cells at the ratio of 1:1 in 24-well plates and treated with GCV (40 μg/ml). Then MDA-MB-231 cells' viability was assessed by Fluc expression at day 1, day 2 and day 3.

2.5. Cell proliferation assay and apoptosis analysis

hUC-MSCs were cultured to 80% confluence, and the supernatant was harvested as hUC-MSCs conditioned medium (MSC-CM) 24 h later and restored at –80 °C until use. To detect the influence of MSC-CM, MDA-MB-231 cells were seeded in a 96-well plate and treated with MSC-CM. Cell proliferation was analyzed by CCK-8 assay at 24 h, 48 h, 72 h after plating. To investigate the influence of hUC-MSC on MDA-MB-231 by direct contact, 1×10^6 hUC-MSCs and 1×10^6 MDA-MB-231 cells were co-cultured in a 6-well plate. The viability of MDA-MB-231 cells was detected by Fluc imaging. In addition, to determine the apoptotic effect of MDA-MB-231 cells stimulated by MSC-CM, MDA-MB-231 cells were cultured with MSC-CM. 48 h later, MDA-MB-231 cells were harvested and then stained using Annexin V and Propidium Iodide (PI) Kit (BD Bioscience) according to the manufacturer's directions. Subsequently, cells were analyzed by FACS.

2.6. Immunofluorescence staining and TUNEL assay

For immunofluorescence staining, rat anti-mouse CD31 antibody (BD Bioscience, Bedford, MA) was used for determining angiogenesis in tumor. Alexa Fluor 594 labeled-secondary antibody (Invitrogen) was used for detection. TUNEL assay was performed using DeadEnd Fluorometric TUNEL System (Promega) according to the manufacturer's directions. Then the sections were stained with 4,6-diamidino-2-phenylindole (DAPI) as counterstaining and observed under a fluorescence microscope.

2.7. Cell migration assay

Transwell migration assays were performed using Transwell chambers with filter membrane of 8 μm pore size (Millipore, Billerica, MA, USA). 1.5×10^4 human umbilical vein endothelial cells (HUVECs) in 200 μl EGM-2 medium (Lonza, Walkersville, MD) were seeded into the inserts with MSC medium or MSC-CM in the lower chamber. After 20 h, non-migrating cells on the upper side of the filter were removed with a cotton swab. Cells migrated were stained with crystal violet and counted at 5 randomly chosen fields at 200 ×.

2.8. Western blotting

For the detection of protein expression, the harvested cells were lysed on ice in a radio-immunoprecipitation assay (RIPA) buffer that included protease inhibitor cocktails. Cell lysates were separated by SDS-PAGE, transferred onto PVDF membrane, and blotted with antibodies against Ki67 (Abcam), caspase-3 (Cell Signaling), cyclin A (Cell Signaling), p-histone H3 (Cell Signaling), Wee1 (Cell Signaling), Myt1 (Cell Signaling), cyclin E2 (Cell Signaling) and β-actin (1:5000, Santa Cruz Biotechnology). The membranes were washed and incubated with horseradish peroxidase-conjugated secondary antibodies (Abcam). Blotting results were detected by an ECL chemiluminescence kit (Millipore, Billerica, MA).

2.9. Real-time RT-PCR

Total RNA was isolated from the cells by TRIzol reagent (Invitrogen) according to the manufacturer's directions. First-strand cDNA was synthesized using oligo dT primers with reverse transcriptase (TransGen Biotech). Subsequently, real-time RT-PCR was performed on Opticon® System (Bio-Rad) in 20 μl reaction volumes. The mRNA expression level of HIF-1a, PDGF-BB, bFGF, PLGF, TGFβ, Ang-1 and Ang-2 was quantified using TransStart Green qPCR SuperMix Kit (TransGen Biotech). The $2^{-\Delta\Delta Ct}$ method was used to determine the relative mRNA folding changes. Primers are listed in Supplemental Table 1.

2.10. Statistical analysis

Statistical analysis was performed using Graphpad Prism 5.0 software (Graph-pad Software Inc., San Diego, CA). Two-way repeated measures ANOVA and two-tailed Student's *t*-test were used. Differences were considered as significant at P values of less than 0.05.

3. Results

3.1. Labeling of cells with reporter genes

For tracking transplanted cells *in vivo*, an imaging assay was developed with reporter genes. Transduction of MDA-MB-231 cells was conducted with double fusion (DF) (Fig. 1A). To obtain cells that can be tracked and also express suicide gene for therapy as well, we transduced hUC-MSCs with renilla luciferase (Rluc), red fluorescence protein (RFP), and herpes simplex virus truncated thymidine kinase (HSV-ttk) (Rluc-RFP-HSV-ttk) triple fusion (TF) reporter gene (Fig. 1B). Immunofluorescence assays revealed that enhanced green fluorescence protein (eGFP) and red fluorescence protein (RFP) were robust expressed on MDA-MB-231 cells and hUC-MSCs-TF (Fig. 1C, D). FACS analysis indicated that GFP and RFP were expressed >95% after sorting (data not shown). In

addition, a strong correlation between Fluc activity and cell numbers was observed in MDA-MB-231 cells, which revealed the availability of assessing tumor growth *in vivo* by analyzing firefly signal intensity. And likewise, the Rluc activity has also showed high correlation with the amount of hUC-MSCs-TF (Fig. 1E, F).

3.2. Effects of hUC-MSCs on tumor growth

To determine the effect of transplanted hUC-MSCs on breast cancer growth, Fluc imaging was introduced to monitor tumor progression. An outline of treatment tumor with hUC-MSCs was showed in Fig. 2A. Breast cancer model was set up by injection of 1×10^6 MDA-MB-231 cells labeled with DF reporter gene into fourth mammary fat pat at both sides of Nu/Nu Nude mice. The tumor bearing mice were divided into 4 groups: (1) control/PBS group, (2) ganciclovir (GCV) group, (3) MSC (hUC-MSC-TF transplantation) group, and (4) MSC + GCV (hUC-MSC-TF transplantation following GCV injection) group. Bioluminescence imaging (BLI) of Fluc was performed to track the development of tumors. After hUC-MSCs-TF transplantation, we found that the tumor growth was inhibited to some extent and this effect can be improved by GCV administration (Fig. 2B). Simultaneously, the survival of hUC-MSCs-TF in tumor was assessed by BLI of Rluc. Those results revealed that the viability of hUC-MSCs-TF was declined continuously over time and the administration of GCV decreased hUC-MSCs-TF survival (Fig. 2C).

3.3. In vivo tumor angiogenesis and apoptosis analysis

To further demonstrate the antitumor effect of transplanted hUC-MSCs, we utilized IntegriSense™ and Annexin-Vivo™ agents for detecting tumor angiogenesis and apoptosis, respectively. After the second cycle of hUC-MSCs-TF transplantation, IntegriSense agent was administrated via intravenous injection and then performed imaging. NIR imaging revealed that the tumor angiogenesis was inhibited in hUC-MSCs-TF treated group and this effect can be enhanced by GCV administration (Fig. 3A). Furthermore, this result was confirmed by immunostaining of CD31 (Fig. 3B). In addition, Annexin-Vivo™ agent was injected intravenously for detecting apoptosis in tumor. NIR imaging showed that the cell apoptosis was promoted in hUC-MSCs-TF treated group and this effect also can be enhanced by GVC application (Fig. 3C). Moreover, this result was confirmed by TUNEL staining (Fig. 3D). Those results suggested that hUC-MSCs could inhibit tumor growth to some extent through decreasing angiogenesis and inducing cell apoptosis.

3.4. Bystander effects of HSV-ttk/GCV suicide system

To test the HSV-ttk suicide system, GCV was added into culture medium and more than 80% of hUC-MSCs-TK cells were killed in the presence of 40 μg/ml GCV (Fig. 4A). In the presence of 40 μg/ml GCV, the toxicity effect reached its maximum degree in 3 days, demonstrating the utility of the HSV-ttk/GCV suicide, and the viability of non-transduced hUC-MSCs kept unaffected (Fig. 4B). To evaluate the bystander effect, we mixed hUC-MSCs-TK and MDA-MB-231 in variable ratio, and 40 μg/ml GCV was given. The cell viability of MDA-MB-231 was evaluated by imaging of Fluc using IVIS imaging system. After 48 h, the viability of MDA-MB-231 cells declined more than 50% in the 2:5, 4:5, 1:1 mixture groups (Fig. 4C). To test the time course effect of HSV-ttk/GCV system, hUC-

MSCs-TF cells were mixed with MDA-MB-231 cells at the ratio of 1:1 and more than 70% of MAD-MB-231 cells were killed in the presence of 40 μg/ml GCV at day 3. By contrast, the MAD-MB-231 cell proliferation was not affected without GCV (Fig. 4D) or with 40 μg/ml GCV without hUC-MSCs-TF cells (data not shown).

3.5. Proliferation effects of hUC-MSCs on MAD-MB-231

To explore the antitumor mechanism of hUC-MSCs, we detected caspase-3 expression in MDA-MB-231 cells treated with hUC-MSC condition medium (MSC-CM). Caspase-3 is an apoptosis-related protein, which will be activated at the end of apoptotic signal pathway. Here, we found there was no obvious difference in the level of activated caspase-3 expression between treated and untreated groups (Fig. 5A). Moreover, the expression of Ki67, a nuclear marker of cell proliferation, was not affected under MSC-CM stimulation (Fig. 5A). Furthermore, treatment of MDA-MB-231 cells with MSC-CM was conducted and FACS analysis results revealed that cell apoptosis of MDA-MB-231 was not affected significantly by hUC-MSCs (Fig. 5B). CCK-8 assay showed that cell proliferation of MDA-MB-231 was inhibited but no obviously change under the treatment of MSC-CM (Fig. 5C). We also found that most of cell cycle regulation proteins have no remarkable change under the treatment of MSC-CM, such as cyclin A, cyclin E2, p-histone H3, Wee1 and Myt1 (Fig. S1). In addition, considering cell proliferation effect affected by cell direct contact, we seeded hUC-MSCs and MDA-MB-231 cells in the same well to make them contact directly. We found that the cell viability of MAD-MB-231 had no remarkable difference compared with MDA-MB-231 cells-only group (Fig. 5D). Taken together, those results indicated that hUC-MSCs have no significant effect on MDA-MB-231 cells proliferation *in vitro*.

3.6. Angiogenic effects of hUC-MSCs

To further investigate the effects hUC-MSC on MAD-MB-231 cells, real time RT-PCR analysis was carried out and the results revealed that angiogenesis-related genes, HIF-1α, bFGF, PECAM-1, PDGF-BB, PLGF, Ang-1, and TGFβ were down-regulated in MDA-MB-231 cells with treatment of MSC-CM (Fig. 6A). Moreover, Transwell assay showed hUC-MSCs significantly suppress the migration of HUVECs (Fig. 6B). Those results indicate that hUC-MSCs can affect tumor vascularization through the release of anti-angiogenic factors and repression of endothelial cells recruitment.

Given the observation of inhibition of tumor growth by intra-tumoral administration of hUC-MSCs, we hypothesized that hUC-MSCs can inhibit tumor angiogenesis and effectively kill nearby tumor cells via the HSV-ttk/GCV suicide system (Fig. 7.

4. Discussion

In this study, we evaluated the interaction between hUC-MSCs and pre-established tumor by dual BLI and NIR imaging. We demonstrated that the transplanted hUC-MSCs played a critical antitumor role *in vivo* in a human breast cancer xenograft model by inhibiting tumor angiogenesis and inducing cell apoptosis. The biodistribution of transplanted hUC-MSCs and therapeutic responses of pre-established tumor can be real-time monitored by firefly and renilla luciferases imaging. Moreover, we observed the therapeutic effects of hUC-MSCs

treatment through inhibiting tumor angiogenesis and inducing cell apoptosis with NIR imaging.

The successful clinical application of future hUC-MSCs transplantation-based tumor therapies needs non-invasive imaging approaches to monitor the fate and tissue distribution of transplanted cells. With the capabilities for visualization, characterization, and measurement of biological processes at the molecular and cellular levels in humans and other living systems, molecular imaging offers the potential for non-invasive assessment therapeutic mechanisms and real-time monitoring of therapeutic responses simultaneously [11,12]. In this study, we investigated the feasibility of using hUC-MSCs as both gene carriers and imaging probes in a breast cancer animal model by transduced with triple fusion reporter gene (RFP-Rluc-HSV-ttk). Moreover, breast cancer cell line MDA-MB-231 cells were transduced with double fusion reporter gene (eGFP-Fluc) for tracking the progression or regression of tumor by Fluc imaging. Fluc and Rluc have different substrates, D-luciferin and coelenterazine respectively [11]. In present study, dual luciferase imaging approach was well established in tracking the transplantation of hUC-MSCs and simultaneously monitoring therapeutic effects *in vivo*. Therefore, the traceable therapeutic strategy provides a versatile platform for exploring multiple approaches for development of new therapies.

In addition to monitoring the therapeutic effects in real time, molecular imaging also is ideally suited to measure *in vivo* tumor biology related to basic molecular and cellular processes such as metabolism, biosynthesis, cell proliferation, and cell death [18]. Tumor growth is angiogenesis-dependent, and therefore vascular imaging would be an effective parameter for monitoring targeted cancer therapy. Angiography-based imaging is considered to be highly suitable for non-invasively visualizing the effect of anti-angiogenesis drug treatment on the structure and function of tumor blood vessels.

One prominent example of peptide ligand is the RGD peptides, which have high affinity to $\alpha v\beta_3$ integrin receptors that are present on the tumor neovasculature and some types of tumor cells [19,20]. Induction of apoptosis is the primary mechanism through which most cancer therapies cause tumor cell death. Early assessment of tumor response is required to better understand the numerous biochemical features after MSCs therapy. With its high affinity for apoptotic cells, lack of immunogenicity, and without *in vivo* toxicity, annexin V has been the most intensively studied imaging probe for *in vivo* apoptosis detection [21]. In this study, we investigated the feasibility of using NIR imaging for tracking tumor angiogenesis and apoptosis after hUC-MSCs administration. We showed that cell death and angiogenesis could be imaged by NIR fluorescence imaging when therapeutic effects could be monitored in real time with bioluminescence imaging simultaneously.

Previous reports revealed that MSCs have an inhibitory effect on tumor proliferation by secreting a number of cytokines such as interleukins, IFN-γ and DKK-1/3 [1]. In this study, hUC-MSCs engineered to express HSV-ttk have been injected into tumor-bearing mice. While inoculation with hUC-MSCs reduced the growth of tumor was observed in vivo and this effect was enhanced by GCV administration, we did not achieve complete tumor regression. We showed that the introduction of a suicide gene into hUC-MSCs could produce a tumor-specific prodrug converting cellular vehicle. In order to provide an initial

assessment of the potential therapeutic index of hUC-MSCs, our current study tested whether these cells could emit regulatory cues to cancer cells *in vitro*. Our findings provide evidence that soluble factors secreted by hUC-MSCs can suppress the angiogenesis pathway and thereby inhibit the proliferation and migration of MDA-MB-231 cells. This is consistent with other reports describing breast cancer inhibitory abilities of MSCs either from bone marrow or umbilical cord through Akt/PI3K and angiogenesis pathways [22,23]. The apparent paracrine findings we describe here may help to introduce a new dimension on the use of hUC-MSCs in cancer therapy.

However, the exact mechanisms by which MSCs might contribute to tumors are controversial. Recent data confirmed that MSCs could play a dual role in cancer progression depending on the cellular context wherein they reside [24,25]. MSC secreted factors, such as CCL5/RANTES, SDF-1, IL-6, and VEGF may accelerate growth of tumor cells upon binding to their respective receptors; however, tumor growth may be inhibited by MSC secreted cytokines such as Dkk-1 [25]. The origins of MSCs should be taken into account when deciding the antitumor effect, as did in the case of hUC-MSCs which inhibit glioblastoma proliferation, but adipose tissue-derived not [26]. Considered the antitumor effect, human MSCs could be more interesting to use for the treatment of pre-established tumors [27]. We speculated that different tissue origin of MSCs, delivery methods, individual variations are key points for future MSCs mediated cancer therapy [25]. With the ability of tropism towards tumor sites, MSCs offer a novel strategy for treating cancer using gene therapy [28–31]. However, the role of MSCs in tumor micro-environment is so complicated that it is very difficult to demonstrate the specific function of MSCs derived different origins in different tumor models. So an extensive understanding about MSCs' function in tumor microenvironment needs to be obtained by further study.

5. Conclusions

Molecular imaging is an invaluable tool in documenting cell delivery, predicting of tumor response to hUC-MSCs therapies and monitoring response to therapy as well as tumor biology, protein expression, and tumor microenvironment. The dual bioluminescence imaging approach provides a versatile platform to monitor tumor progression and hUC-MSCs simultaneously within the same animal. Consequently, therapeutic effects also could be monitored in real time with molecular imaging simultaneously.

Supplementary Material

Refer to Web version on PubMed Central for supplementary material.

Acknowledgments

Funding: This work was partially supported by grants from the National Basic Research Program of China (2011CB964903, 2013CB967201), National Natural Science Foundation of China (81320108014, 81371620), Program for New Century Excellent Talents in University (NCET-12-0282), Tianjin Natural Science Foundation (12JCZDJC24900), and the Innovation Program of Nankai University for Undergraduates in 2012 (121005523).

References

1. Kucerova L, Matuskova M, Hlubinova K, Altanerova V, Altaner C. Tumor cell behaviour modulation by mesenchymal stromal cells. Mol Cancer. 2010; 9:129. [PubMed: 20509882]
2. Yong RL, Shinojima N, Fueyo J, Gumin J, Vecil GG, Marini FC, et al. Human bone marrow-derived mesenchymal stem cells for intravascular delivery of oncolytic adenovirus Δ24-RGD to human gliomas. Cancer Res. 2009; 69:8932–40. [PubMed: 19920199]
3. Kidd S, Caldwell L, Dietrich M, Samudio I, Spaeth EL, Watson K, et al. Mesenchymal stromal cells alone or expressing interferon-β suppress pancreatic tumors *in vivo*, an effect countered by anti-inflammatory treatment. Cytotherapy. 2010; 12:615–25. [PubMed: 20230221]
4. Nakamizo A, Marini F, Amano T, Khan A, Studeny M, Gumin J, et al. Human bone marrow-derived mesenchymal stem cells in the treatment of gliomas. Cancer Res. 2005; 65:3307–18. [PubMed: 15833864]
5. Mader EK, Maeyama Y, Lin Y, Butler GW, Russell HM, Galanis E, et al. Mesenchymal stem cell carriers protect oncolytic measles viruses from antibody neutralization in an orthotopic ovarian cancer therapy model. Clin Cancer Res. 2009; 15:7246–55. [PubMed: 19934299]
6. Josiah DT, Zhu D, Dreher F, Olson J, McFadden G, Caldas H. Adipose-derived stem cells as therapeutic delivery vehicles of an oncolytic virus for glioblastoma. Mol Ther. 2009; 18:377–85. [PubMed: 19904233]
7. Dwyer RM, Khan S, Barry FP, O'Brien T, Kerin MJ. Advances in mesenchymal stem cell-mediated gene therapy for cancer. Stem Cell Res Ther. 2010; 1:25. [PubMed: 20699014]
8. Fillat C, Carrio M, Cascante A, Sangro B. Suicide gene therapy mediated by the herpes simplex virus thymidine kinase gene/ganciclovir system: fifteen years of application. Curr Gene Ther. 2003; 3:13–26. [PubMed: 12553532]
9. Su W, Wang L, Zhou M, Liu Z, Hu S, Tong L, et al. Human embryonic stem cell-derived endothelial cells as cellular delivery vehicles for treatment of meta-static breast cancer. Cell Transplant. 2013; 22:2079–90. [PubMed: 23067802]
10. Zhou M, Wang L, Su W, Tong L, Liu Y, Fan Y, et al. Assessment of therapeutic efficacy of liposomal nanoparticles mediated gene delivery by molecular imaging for cancer therapy. J Biomed Nanotechnol. 2012; 8:742–50. [PubMed: 22888744]
11. Wang L, Su W, Liu Z, Zhou M, Chen S, Chen Y, et al. CD44 antibody-targeted liposomal nanoparticles for molecular imaging and therapy of hepatocellular carcinoma. Biomaterials. 2012; 33:5107–14. [PubMed: 22494888]
12. Wang L, Wang Y, Li Z. Nanoparticle-based tumor theranostics with molecular imaging. Curr Pharm Biotechnol. 2013; 14:683–92. [PubMed: 24372235]
13. Weissleder R. Molecular imaging in cancer. Science. 2006; 312:1168–71. [PubMed: 16728630]
14. Keren S, Zavaleta C, Cheng Z, de la Zerda A, Gheysens O, Gambhir SS. Noninvasive molecular imaging of small living subjects using Raman spectroscopy. Proc Natl Acad Sci U S A. 2008; 105:5844–9. [PubMed: 18378895]
15. Yang ZX, Han ZB, Ji YR, Wang YW, Liang L, Chi Y, et al. CD106 identifies a subpopulation of mesenchymal stem cells with unique immunomodulatory properties. PLoS One. 2013; 8:e59354. [PubMed: 23555021]
16. Wang Y, Zhang Z, Chi Y, Zhang Q, Xu F, Yang Z, et al. Long-term cultured mesenchymal stem cells frequently develop genomic mutations but do not undergo malignant transformation. Cell Death Dis. 2013; 4:e950. [PubMed: 24309937]
17. Li Z, Wilson KD, Smith B, Kraft DL, Jia F, Huang M, et al. Functional and transcriptional characterization of human embryonic stem cell-derived endothelial cells for treatment of myocardial infarction. PLoS One. 2009; 4:e8443. [PubMed: 20046878]
18. Specht JM, Mankoff DA. Advances in molecular imaging for breast cancer detection and characterization. Breast Cancer Res. 2012; 14:206. [PubMed: 22423895]
19. Ruoslahti E. RGD and other recognition sequences for integrins. Annu Rev Cell Dev Biol. 1996; 12:697–715. [PubMed: 8970741]

20. Schiffelers RM, Koning GA, ten Hagen TL, Fens MH, Schraa AJ, Janssen AP, et al. Anti-tumor efficacy of tumor vasculature-targeted liposomal doxorubicin. J Control Release. 2003; 91:115–22. [PubMed: 12932643]
21. Niu G, Chen X. Apoptosis imaging: beyond annexin V. J Nucl Med. 2010; 51:1659–62. [PubMed: 20956479]
22. Ho IA, Toh HC, Ng WH, Teo YL, Guo CM, Hui KM, et al. Human bone marrow-derived mesenchymal stem cells suppress human glioma growth through inhibition of angiogenesis. Stem Cells. 2013; 31:146–55. [PubMed: 23034897]
23. Ma Y, Hao X, Zhang S, Zhang J. The in vitro and in vivo effects of human umbilical cord mesenchymal stem cells on the growth of breast cancer cells. Breast Cancer Res Treat. 2012; 133:473–85. [PubMed: 21947651]
24. Klopp AH, Gupta A, Spaeth E, Andreeff M, Marini F. Concise review: dissecting a discrepancy in the literature: do mesenchymal stem cells support or suppress tumor growth? Stem Cells. 2011; 29:11–9. [PubMed: 21280155]
25. Torsvik A, Bjerkvig R. Mesenchymal stem cell signaling in cancer progression. Cancer Treat Rev. 2013; 39:180–8. [PubMed: 22494966]
26. Akimoto K, Kimura K, Nagano M, Takano S, To'a Salazar G, Yamashita T, et al. Umbilical cord blood-derived mesenchymal stem cells inhibit, but adipose tissue-derived mesenchymal stem cells promote, glioblastoma multiforme proliferation. Stem Cells Dev. 2013; 22:1370–86. [PubMed: 23231075]
27. Keramidas M, de Fraipont F, Karageorgis A, Moisan A, Persoons V, Richard MJ, et al. The dual effect of mesenchymal stem cells on tumour growth and tumour angiogenesis. Stem Cell Res Ther. 2013; 4:41. [PubMed: 23628074]
28. Martinez-Quintanilla J, Bhere D, Heidari P, He D, Mahmood U, Shah K. Therapeutic efficacy and fate of bimodal engineered stem cells in malignant brain tumors. Stem Cells. 2013; 31:1706–14. [PubMed: 23389839]
29. Keung EZ, Nelson PJ, Conrad C. Concise review: genetically engineered stem cell therapy targeting angiogenesis and tumor stroma in gastrointestinal malignancy. Stem Cells. 2013; 31:227–35. [PubMed: 23132810]
30. Dai, LJ.; Sun, XY.; Luo, J.; Warnock, GL. Mesenchymal stem cells: prospects for cancer therapy. In: Danquah, MK.; Mahato, RI., editors. Emerging trends in cell and gene therapy. New York: Humana Press; 2013. p. 271-86.
31. Khakoo AY, Pati S, Anderson SA, Reid W, Elshal MF, Rovira II, et al. Human mesenchymal stem cells exert potent antitumorigenic effects in a model of Kaposi's sarcoma. J Exp Med. 2006; 203:1235–47. [PubMed: 16636132]

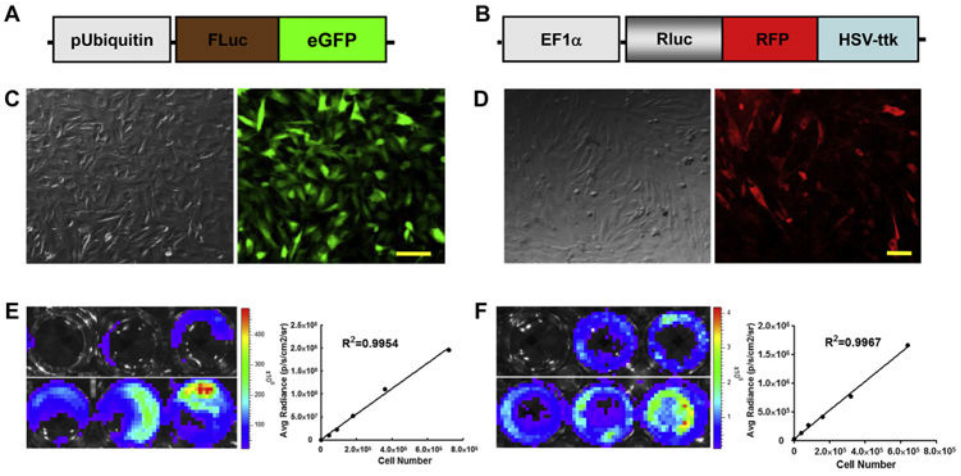

Fig. 1.

Transduction of MAD-MB-231 cells, hUC-MSCs with double fusion (DF) and triple fusion (TF) reporter genes, respectively. (A) Schema of the DF reporter gene containing Fluc and eGFP driven by an ubiquitin promoter. (B) Schema of the TF reporter gene contains Rluc-RFP-HSV-ttk driven by an EF-1α promoter. (C) Transduced MDA-MB-231 cells are strongly positive for eGFP on fluorescence microscopy. (D) RFP was expressed robustly in hUC-MSCs. (E & F) *Ex vivo* imaging analysis of stably transduced MDA-MB-231 cells and hUC-MSCs shows a robust correlation between cell numbers and Fluc/Rluc reporter gene activity. Scale bar = 100 μm.

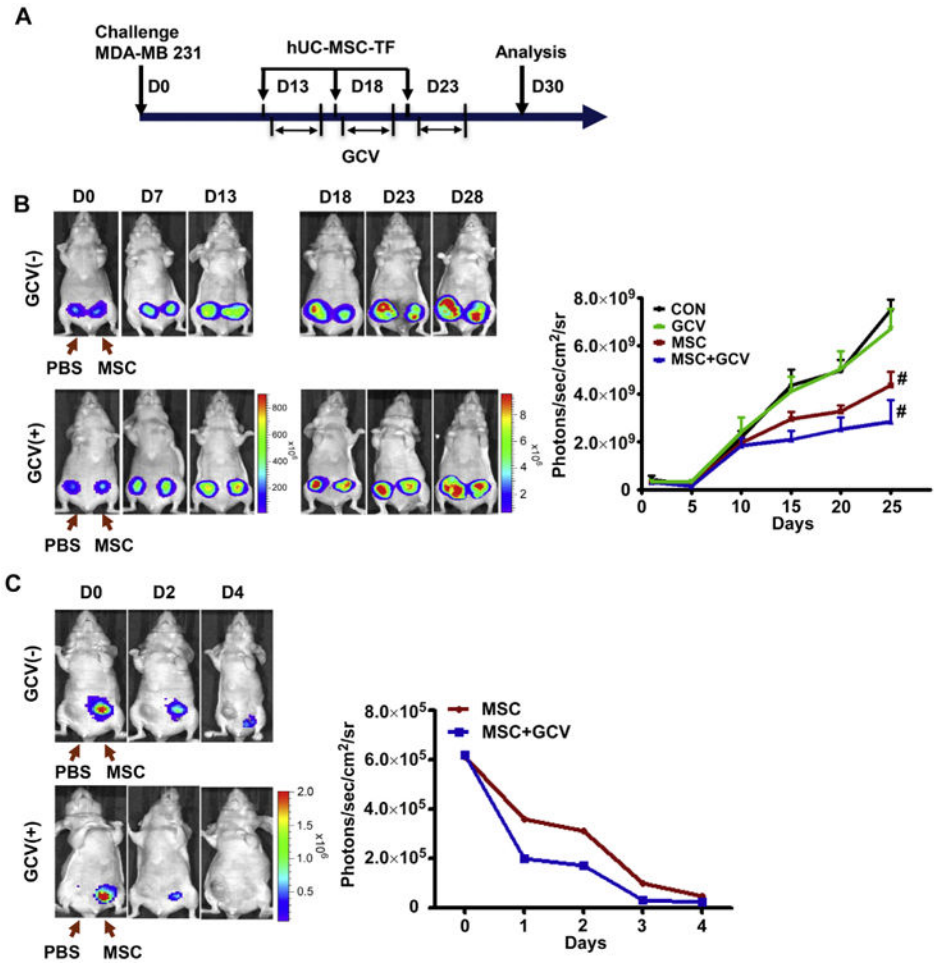

Fig. 2.

In vivo inhibition of tumor growth by hUC-MSCs via HSV-ttk system. (A) Schema of treatment of breast cancer with hUC-MSC-TF cells. (B) Firefly luciferase (Fluc) imaging of tumor progression (left). Quantitative analysis of Fluc signal (right). (C) Renilla luciferase (Rluc) imaging of hUC-MSCs-TF from day 0 to day 4 in the second cycle of hUC-MSCs administration (left). Quantitative analysis of Rluc signal. Bioluminescence activity is showed as photons/s/cm^2/sr. #$P < 0.01$ compared to control.

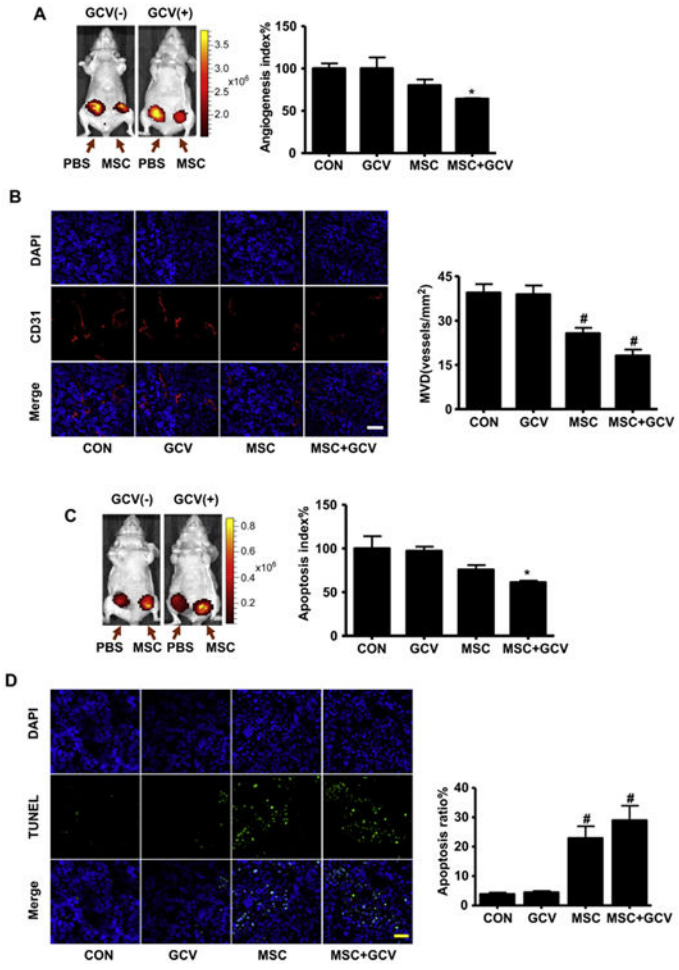

Fig. 3.

In vivo reduction of tumor angiogenesis and enhancement of cell apoptosis by hUC-MSCs. (A) Near infrared fluorescence (NIR) imaging of integrin $\alpha v\beta_3$ activity after two consecutive hUC-MSCs administration via injection of IntegriSense™. Angiogenesis index was indicated by relative radiance compare to the control group. (B) Representative CD31 staining of tumor sections from each group. Quantitative analysis of capillary density was significantly lower in the hUC-MSCs and hUC-MSCs/GCV groups compared with the control and GCV groups. (C) Representative images after hUC-MSCs administration by intravenous injection of Annexin-Vivo™. Apoptosis index was indicated by relative radiance compared to the control group. (D) Apoptosis was measured by the TUNEL assay. Quantitative analysis of TUNEL assay. Tumor cell apoptosis was promoted in hUC-MSCs-TF treated group and this effect can be enhanced by GVC application. Scale bar = 50 μm. $^{*}P < 0.05$, $^{\#}P < 0.01$ compared to control.

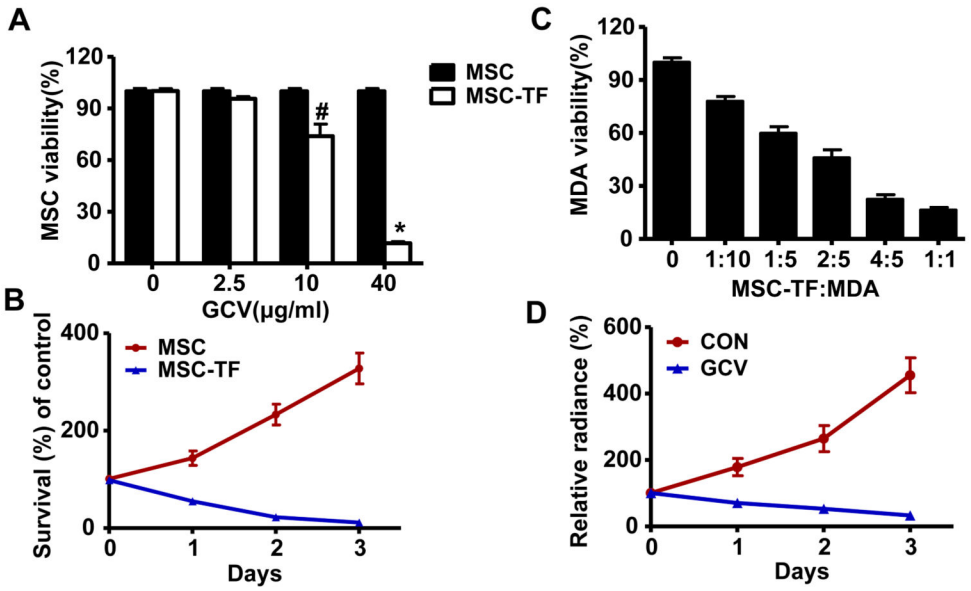

Fig. 4.

hUC-MSCs-TF exhibit a great sensitivity to prodrug GCV and bystander effect on MDA-MB-231 cells *in vitro*. (A) hUC-MSCs or hUC-MSC-TF cells were plated and treated with increasing concentrations of GCV, and viability of cells was measured 2 days later. (B) hUC-MSCs or hUC-MSC-TF cells were cultured with GCV (40 μg/ml) for 3 days, and cell viability was measured by CCK-8 assay every day. (C) Mixtures of hUC-MSC-TF and MDA-MB-231 cells in the ratios (hUC-MSC-TF: MDA-MB-231=0, 1:10, 1:5, 2:5, 4:5, 1:1) were treated with GCV (40 μg/ml) for 48 h, and the viability of MDA-MB-231 cells was indicated by the relative radiance compared to 0% group by imaging Fluc activity in MDA-MB-231 cells. (D) Mixtures of hUC-MSC-TF cells and the same number of MDA-MB-231 cells were treated with PBS or GCV (40 μg/ml) for 3 days. The cell viability of MDA-MB-231 was measured as mentioned above. More than 70% of MAD-MB-231 cells were killed in the presence of 40 μg/ml GCV at day 3, but the cell proliferation was not affected without GCV. $^{\#}P < 0.05$, $^{*}P < 0.01$ compared to control. Note: MSC, hUC-MSC; MSC-TF, hUC-MSC-TF; MDA, MDA-MB-231.

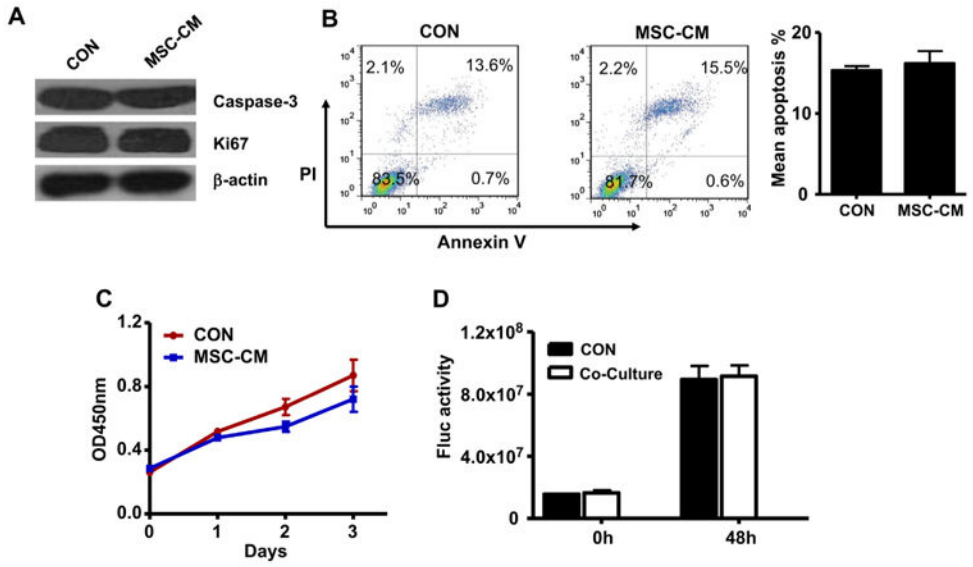

Fig. 5.

hUC-MSCs have no significant effect on MDA-MB-231 cell proliferation *in vitro*. (A) Expression of proliferation marker Ki67 and apoptosis marker cleaved caspase-3 in MDA-MB-231 cells was not affected by MSC-CM. (B) FACS analysis of MDA-MB-231 cells treated with MSC-CM was conducted by staining MAD-MB-231 with Annexin V and PI (Propidium Iodide). Quantitative analysis results revealed that the cell apoptosis of MAD-MB-231 was not affected significantly by hUC-MSCs. (C) The cell proliferation of MDA-MB-231 was inhibited MSC-CM, but no significant difference. (D) The viability of MDA-MB-231 cells was not affected by hUC-MSCs through direct contact.

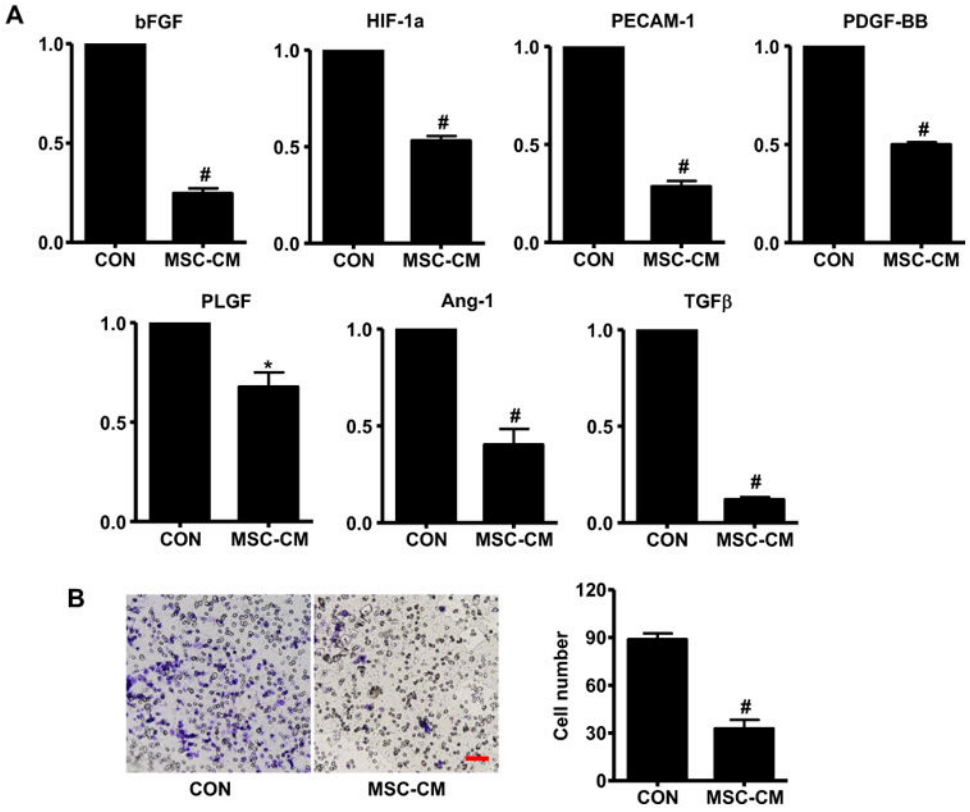

Fig. 6.

hUC-MSCs down-regulate the expression of angiogenic factors in MAD-MB-231 cells and inhibit endothelial cell migration. (A) Analysis of angiogenic factors expression in MDA-MB231 treated with MSC-CM. (B) Representative photographs of Transwell assay of HUVECs treated with MSC-CM. Quantitative analysis results revealed that the migration of HUVECs was significantly suppressed by hUC-MSCs. Scale bar = 100 μm. $^{*}P < 0.05$, $^{\#}P < 0.01$ compared to control.

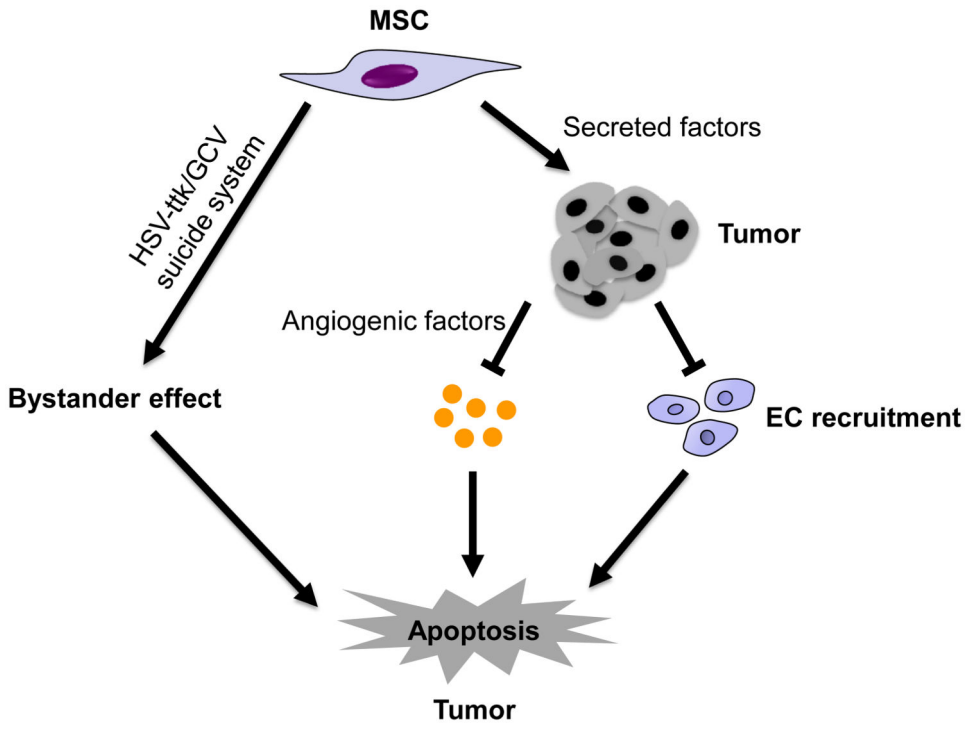

Fig. 7.

Putative model outlining the tumor-suppressive effects of hUC-MSCs by inhibiting tumor angiogenesis or inducing tumor cell death through bystander effect via the HSV-ttk/GCV suicide system. EC, endothelial cell.